Weierstraß-Institut

für Angewandte Analysis und Stochastik

Leibniz-Institut im Forschungsverbund Berlin e. V.

Preprint ISSN 0946 – 8633

Sensitivity analysis of 2D photonic band gaps of any rod shape and conductivity using a very fast conical integral equation method

Leonid Goray[1], Gunther Schmidt[2]

submitted: February 8, 2012

[1] St. Petersburg Academic University
Khlopina 8/3
St. Petersburg 194021
and
Institute for Analytical Instrumentation, RAS
Rizhsky Prospect 26
St. Petersburg 190103
Russian Federation
E-Mail: lig@pcgrate.com

[2] Weierstrass Institute
Mohrenstr. 39
10117 Berlin
Germany
E-Mail: gunther.schmidt@wias-berlin.de

No. 1684
Berlin 2012

2008 *Physics and Astronomy Classification Scheme.* 02.60.Nm, 02.70.Pt, 71.36.+c.

Key words and phrases. Diffraction, multilayer periodic structure, integral method, oblique incidence,photonic crystal grating, S-matrix method.

Edited by
Weierstraß-Institut für Angewandte Analysis und Stochastik (WIAS)
Leibniz-Institut im Forschungsverbund Berlin e. V.
Mohrenstraße 39
10117 Berlin
Germany

Fax: +49 30 2044975
E-Mail: preprint@wias-berlin.de
World Wide Web: http://www.wias-berlin.de/

ABSTRACT. The conical boundary integral equation method has been proposed to calculate the sensitive optical response of 2D photonic band gaps (PBGs), including dielectric, absorbing, and high-conductive rods of various shapes working in any wavelength range. It is possible to determine the diffracted field by computing the scattering matrices separately for any grating boundary profile. The computation of the matrices is based on the solution of a 2×2 system of singular integral equations at each interface between two different materials. The advantage of our integral formulation is that the discretization of the integral equations system and the factorization of the discrete matrices, which takes the major computing time, are carried out only once for a boundary. It turned out that a small number of collocation points per boundary combined with a high convergence rate can provide adequate description of the dependence on diffracted energy of very different PBGs illuminated at arbitrary incident and polarization angles. The numerical results presented describe the significant impact of rod shape on diffraction in PBGs supporting polariton-plasmon excitation, particularly in the vicinity of resonances and at high filling ratios. The diffracted energy response calculated vs. array cell geometry parameters was found to vary from a few percent up to a few hundred percent. The influence of other types of anomalies (i.e. waveguide anomalies, cavity modes, Fabry-Perot and Bragg resonances, Rayleigh orders, etc), conductivity, and polarization states on the optical response has been demonstrated.

1. INTRODUCTION

In the recent two decades, we have been witnessing exponentially growing interest, both of theoreticians and experimenters, in the properties of photonic band gaps (PBGs) and metamaterials. Progress in the technology of nanostructures with a characteristic surface relief size of the order of 10–100 nm has stimulated production of two- and three-dimensional periodic structures with periods shorter than the wavelength λ of visible light, i.e. sub-wavelength diffraction gratings. Nowadays considerable effort is devoted to the investigation of polariton-plasmon PBGs with metallic or semiconducting nanostructures supporting strong light-matter interaction. Large photonic band gaps, extraordinary light transmission properties, negative refraction, and strong coupling between the electronic and photonic resonances can be supported in such structures. Though surface plasmon excitation plays a predominant part in metallic sub-wavelength PBGs, other types of electromagnetic resonances can also exist in complex material structures working in different wavelength ranges: Rayleigh anomalies, Fabry-Perot and Bragg resonances, waveguiding anomalies, cavity modes, etc. In some cases it is difficult to distinguish among these phenomena, owing to their gradual mutation from one into another, and determine which is which even using electromagnetic field map distributions inside the slab structure. There is therefore a growing need for methods based on a rigorous theory which would be universal, accurate and fast enough.

Numerical methods are ordinarily employed in treating diffracting structures whose characteristic dimensions (more specifically, period d, slab (rod) width l, depth h, correlation length, etc) are comparable with the wavelength of the incident radiation ($\lambda/d \sim 1$), i.e., in the resonance region. Structures with sub-wavelength dimensions require solution of the problem in terms of electromagnetic theory, in other words, of Maxwell's equations with rigorous boundary conditions and radiation conditions [1]. A wide range of various techniques that have been developed for the analysis of some kinds of gratings may also be used for PBG analysis [2]. Theory offers presently rigorous numerical methods to solve problems of diffraction from multi-boundary 1D and 2D gratings with arbitrary groove profiles, which can conveniently be assigned to two branches, integral or differential, of electromagnetic theory. The first of them includes, again by convention only, methods involving finite elements (including boundary or volume, time or frequency domain), fictitious sources, and integral equations (boundary or volume). Some methods resembling closely the differential approach, among them the modal (sometimes referred to as characteristic-wave or characteristic-modal) method, coupled-wave (Fourier-modal) method, and method of coordinate transformation are classed by some researchers

among a special group [3, 4]. They all are based essentially on Maxwell's equations in partial derivatives. In a general case, differential theory includes typically integration of these equations over one or two coordinates. Most of the currently used differential methods resort to one-dimensional integration or some other numerical approach in solving a system of conventional differential equations. The method of boundary integral equations treats Maxwell's equations in the integro-differential form, with their subsequent numerical solution by curvilinear integration. Some versions of the finite-element method can also be assigned to the integral theory. In contrast to the method of integral equations, this approach assumes, as a rule, two-dimensional integration, the only exclusion being the method of boundary integral elements. Drawing basically close to the method of integral equations is that of fictitious sources [2]. For a comprehensive review of a large number of theoretical treatments and their mathematical realizations, the Reader is referred to the above mentioned books and references therein.

An approach most frequently followed when considering scattering from ordered or partially ordered objects like PBGs is the straightforward and readily tractable plane wave expansion (PWE) method [5]. Although a plethora of more or less universal and effective rigorous analyses exists, this is a good introduction to the business of band diagrams and is probably the easiest method to understand [6]. It is well known that this method suffers from poor convergence for metallic gratings and needs large computation times, especially for the TM-polarized incident light, because of its main accuracy parameter scaling cubically with time [7, 8]. In the theoretical investigations applied to diffraction gratings this approach is well known as the rigorous coupled-wave analysis (CWA). We are going to dwell on it in some detail to be able to compare its advantages and shortcomings with the method of boundary integral equations employed by the present authors in treating the PBGs and other grating problems. In many problems of diffraction monochromatic light is used and analysis of these problems requires solution of the scalar or vector Helmholtz equation (in its wave form). If we restrict ourselves to consideration of periodic objects only, for example, to 1D or 2D diffraction gratings, and 2D or 3D photonic crystals, this method will turn out particularly appropriate for operation with the Helmholtz equation. The first to apply it, albeit not in a rigorous formulation, to analysis of volume holograms was Kogelnik in as far back as 1969. M. Moharam and T. Gaylord applied the coupled wave method to analysis of diffraction gratings in its rigorous formulation, at any rate, to gratings with lamellar (rectangular) profile in 1981 [9]. The CWA treats the electromagnetic field $u(x, y)$ in homogeneous regions of space, in front of a periodic object and behind it, as comprised of a linear combination of plane waves. For a non-periodic confined object one has to accept, in place of a linear combination of plane waves, a continuous expansion in plane waves in the form of the Fourier integral. In the region of the object, Maxwell's equations are solved by Fourier transformation. To find the unknown coefficients in the Fourier expansions, a system of linear algebraic equations is formulated. Application of the CWA to classical 2D diffraction problems with 1D-periodic boundaries, i.e., with a stepwise changing dielectric and/or magnetic permeability at the boundary is essentially different for the TE and TM cases (with the electric vector confined to the plane perpendicular to the plane of the incident wave vector $\mathbf{k}$ and parallel to the grating grooves, or lying in the $\mathbf{k}$ plane, respectively). In the case of the TE polarization, the unknown electromagnetic field and its normal derivative remain continuous at the boundary. For the TM polarization, the normal derivative suffers a discontinuity, which is responsible for all subsequent problems associated with convergence and accuracy of the method, a factor that nobody has yet found a way to combat. While the CWA intuitively appears to be tractable, the present authors are unaware of any mathematical publications which would offer a rigorous substantiation of its convergence, even for a smooth wavenumber $k(x, y)$ relation. The main difficulty standing in the way of such a substantiation is the exponential growth of the elements of transmission matrices along the rows and columns [4]. This growth gives rise to numerical problems; matrices and the corresponding systems of differential equations are poorly conditioned; indeed, their eigenvalues belong to different scales, and this effect is the stronger, the more harmonics are taken into account [10]. Obviously enough,

diffraction problems with a discontinuity of k at the interfaces will meet with the natural constraint on the convergence rate for the CWA. Indeed, the Fourier coefficients of $k^2(x, y)$ and $u(x, y)$ cannot approach zero fast enough for the $y = const$ line which crosses the boundary. The best version of factorization available thus far for the CWA and other similar methods of the differential group in the TM polarization called Fast Fourier Factorization [4], enjoys presently wide recognition. Its authors have, however, revealed the remaining above mentioned limitations of a fundamental nature which place a constraint on the use of this approach in cases of high conductivity in the TM polarization [11]. Besides, application of the CAW to non-lamellar profiled gratings involves discretization into plane layers, the so-called staircase approximation. This approximation was shown not to be rigorous [12]; indeed, as the number of the layers increases, the result obtained in solution of the equations will not necessarily tend to accurate values. In the case of the TE polarization and 1D gratings, the convergence of this approximation is, as a rule, good, but in the TM case an increase in the number of layers does not improve the results; on the contrary, they begin to diverge. This can also be seen from an analysis of the properties of the solution in the case of one layer and TM polarization [13]. The conclusions drawn for the case of 2D diffraction from 1D gratings with one boundary will naturally hold for multi-boundary gratings, conical (3D) diffraction and bi-periodic gratings. Nevertheless, for lack of a better alternative, the CWA is widely used for 1D and 2D gratings in micro-optics analysis and waveguide technology, as well as in problems involving synthesis, for instance, of multi-order diffraction gratings or diffraction optical elements (DOEs) with preset characteristics [14].

The method of boundary integral equations (briefly – IM) is presently universally recognized as one of the most developed and flexible approaches to accurate numerical solution of diffraction grating problems (cf. Refs. [1, 15, 16] and references therein). Viewed in the historical context, this method was the first to offer a solution to vector problems of light diffraction by optical gratings with a high enough accuracy, and to demonstrate remarkable agreement with experimental data [3, 17]. This should be attributed to the high accuracy and good convergence of the method, especially for the TM polarization plane [16, 18]. It does not involve limitations similar to those characteristic of the CWA, and it provides a better convergence. To disadvantages of this method belong its being mathematically complicated, as well as numerous "peculiaritiesïnvolved in numerical realization. Besides, application of the IM to cases of heterogeneous or anisotropic media meets with difficulties, however with the volume integral method it is possible to overcome such difficulties. Nevertheless, it is on the basis of this theory that all the well-known problems of diffraction by periodic and non-periodic structures in optics and other fields have been solved. In many cases it offers the only possible way to follow in research [3, 19, 20]. The flexibility and universality inherent in the IM, in particular, enable one rather easily to reduce the problem of radiation of Gaussian waves or of a localized source to that of plane wave incidence, for which scientists all over the world have a set of numerical solutions. Generalizations of the IM have been recently proposed for: arbitrarily profiled 1D multi-layer gratings [21]; randomly rough x-ray-extreme-UV mirrors [22]; conical diffraction gratings including materials with negative permittivity and permeability [18, 23, 24]; arbitrarily rough multi-layer 1D gratings and mirrors [25]; bi-periodic anisotropic structures using a variation formulation [26]; Fresnel zone plates and DOEs [27, 28]; 3D PBGs of some geometries using volume [7] and surface [29] integrals, etc. The motivation for the present work is to introduce the new method as an exact and universal approach to be applied in areas where rapid design and analysis of the most sensitive PBGs cases would be at a premium. The corresponding theory is described in Section 2. The diffraction problem and boundary relations between values of the fields across the boundary are formulated in Subsection 2.1. The method of scattering amplitude matrices (S-matrix algorithm) expedient for the calculation of far-fields and polarization properties of conical diffraction by PBGs is described in Subsection 2.2. The respective integral equations in terms of boundary potentials can be found in Subsection 2.3. Numerical implementation of the developed theory is described briefly in Section 3. Diverse numerical tests devoted to application of the method and obtaining results for sensitive cases of various PBGs are given in Section 4. In Subsection 4.1

we compare our results with data obtained by the other well-established approach and give examples of the significant impact of rod shape and filling ratio on diffraction in metallic PBGs supporting the polariton-plasmon excitation, particular close to resonances. In Subsection 4.2 we demonstrate the influence of high conductivity on transmission spectra of lossless PBGs supporting waveguide modes at different polarization states. In Subsection 4.3 we calculate transmission spectra of dielectric PBGs supporting Bragg resonances in conical diffraction.

2. THEORY

We employed the IM for a theoretical description of the optical properties of PBGs. The theory of diffraction on separated boundaries is covered here necessarily on the whole because its main parts including mathematical aspects have been derived at considerable length in Refs. 18, 24, 28, 30, 31. The electromagnetic formulation of diffraction by gratings, which are modeled as infinite periodic structures, can be reduced to a system of Helmholtz equations for the z-components of the electric and magnetic fields in $\mathbb{R}^2$, where the solutions have to be quasi-periodic in the x-direction, subject to radiation conditions in the y-direction, and satisfy certain jump conditions at the interfaces between different materials of the diffraction grating. In the case of classical diffraction, when $\mathbf{k}$ is orthogonal to the z-direction, the system splits into independent problems for the two basic polarizations of the incident wave, whereas in the case of conical diffraction (Fig. 1) the boundary values of the field z-components, as well as their normal and tangential derivatives at the interfaces, are coupled. Thus the unknowns are scalar functions in the case of classical diffraction, and two-component vector functions in the conical case. A grating diffracts the incoming plane wave into a finite number of outgoing plane waves, the so-called reflected and transmitted modes or orders. The program computes the energies and polarizations of these modes for an arbitrary number of layers with different boundary profile types including closed boundary profiles (i.e. inclusions). The boundary profiles of the layers must be strictly separated, i.e. the maximal y-value of a given profile is strictly less than the minimal y-value of the next profile above. In this case, it is possible to determine the diffracted field of the grating by computing scattering amplitude matrices separately for any profile. For each interface between two different materials the computation of the scattering amplitude matrices corresponds to solving one-boundary conical diffraction problems with plane waves illuminating the interface from above and below. Using the integral method one has to solve for each interface a 2×2 system of singular integral equations with different right-hand sides. The equations are discretized with a collocation method, the unknowns are sought as trigonometric polynomials which in the case of profiles with edges are partially replaced by splines to improve the approximation of the solution near the edges.

2.1. **Diffraction problem.** In the multi-boundary diffraction problem one has to deal with cylindrical surfaces $\Sigma_n \times \mathbb{R}$, $n = 0, ..., N-1$, either open or closed, which are d-periodic in x and whose generatrices are parallel to the z-axis (Fig. 2). The surfaces separate $N+1$ periodic regions $G_n \times \mathbb{R}$,

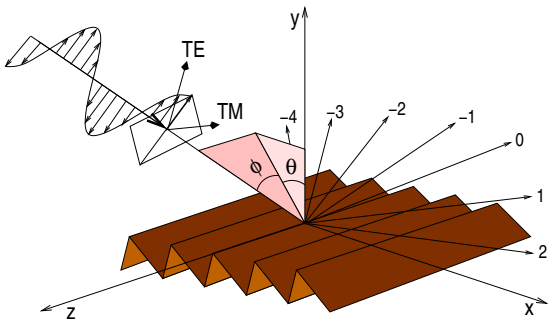

FIGURE 1. Schematic conical diffraction by a grating.

filled with material of constant permittivity and permeability. The grating structure is characterized by piecewise constant functions of electric permittivity ε and magnetic permeability μ, which are d-periodic in x, homogeneous in z, and have jumps at the surfaces Σ_n. The values of these functions in the semi-infinite regions $G_0 \times \mathbb{R}$ above and $G_N \times \mathbb{R}$ below the inhomogeneous structure are denoted by ε_0, μ_0 and ε_N, μ_N, respectively. We assume that $\lambda = 2\pi c/\omega$ with a light velocity c at a given pulsatance ω and the incident time-harmonic field with polarization vectors $\mathbf{p}$ and s defined later is given by

$$(\mathbf{E}^i, \mathbf{H}^i) = (\mathbf{p}, \mathbf{s})\mathrm{e}^{\,\mathrm{i}\omega t}\mathrm{e}^{\,\mathrm{i}(\alpha x - \beta y + \gamma z)},$$

where $(\alpha, -\beta, \gamma) = \omega\sqrt{\varepsilon_0\mu_0}(\sin\theta\cos\phi, -\cos\theta\cos\phi, \sin\phi)$, and $|\theta|, |\phi| < \pi/2$. Due to the periodicity of the surfaces the incident wave is scattered into a finite number of plane waves in $G_0 \times \mathbb{R}$ and also in $G_N \times \mathbb{R}$ if $\varepsilon_N\mu_N > 0$. The wave vectors of these outgoing orders lie on the surface of a cone whose axis is parallel to the z-axis. Therefore one speaks of conical diffraction. Classical diffraction corresponds to $\gamma = 0$, whereas $\gamma \neq 0$ characterizes conical diffraction. Using the representation of the total field $\mathbf{E}(x, y, z) = E(x, y)\mathrm{e}^{\,\mathrm{i}\gamma z}$, $\mathbf{H}(x, y, z) = \sqrt{\varepsilon_0/\mu_0}B(x, y)\mathrm{e}^{\,\mathrm{i}\gamma z}$ the system of time-harmonic Maxwell equations transforms to 2D Helmholtz equations in the domains G_n, where ε and μ are constant,

$$(\Delta + (\omega\kappa)^2)\, E(x, y) \,= (\Delta + (\omega\kappa)^2)\, B(x, y) \,= 0 \tag{1}$$

with the coefficient function $(\omega\kappa)^2 = \omega^2\varepsilon\mu - \gamma^2$ piecewise constant and d-periodic in x.

It can be shown that under the condition $\kappa \neq 0$, which will be assumed throughout, the z-components E_z, B_z of the vector functions E and B determine the total electromagnetic field $(\mathbf{E}, \mathbf{H})$. The continuity of the tangential components of $\mathbf{E}$ and $\mathbf{H}$ on the surface Σ_n implies jump conditions for E_z, B_z in the form (see Ref. 18)

$$\begin{gathered} \big[E_z\big]_{\Sigma_n} = \big[H_z\big]_{\Sigma_n} = 0, \\ \Big[\frac{\varepsilon\,\partial_\nu E_z}{\kappa^2}\Big]_{\Sigma_n} = -\varepsilon_0 \sin\phi \Big[\frac{\partial_t B_z}{\kappa^2}\Big]_{\Sigma_n}, \; \Big[\frac{\mu\,\partial_\nu B_z}{\kappa^2}\Big]_{\Sigma_n} = \mu_0 \sin\phi \Big[\frac{\partial_t E_z}{\kappa^2}\Big]_{\Sigma_n}, \end{gathered} \tag{2}$$

where $[.]$ denotes the jump of functions on Σ_n, and $\partial_\nu = \nu_x\partial_x + \nu_y\partial_y$ and $\partial_t = -\nu_y\partial_x + \nu_x\partial_y$ are the normal and tangential derivatives on Σ_n, respectively. The z-components of the incoming field

$$E_z^i(x, y) = p_z\mathrm{e}^{\,\mathrm{i}(\alpha x - \beta y)},\; B_z^i(x, y) = s_z\mathrm{e}^{\,\mathrm{i}(\alpha x - \beta y)}\sqrt{\mu_0/\varepsilon_0} = q_z\mathrm{e}^{\,\mathrm{i}(\alpha x - \beta y)}$$

are α-quasiperiodic in x of period d. Here the vector s is orthogonal to the plane spanned by $\mathbf{k}$ and the grating normal $\nu = (0, 1, 0)$ and $\mathbf{p}$ lies in that plane:

$$\mathbf{s} = \mathbf{k} \times (0, 1, 0)/|\mathbf{k} \times (0, 1, 0)|,\; \mathbf{p} = \mathbf{s} \times \mathbf{k}/|\mathbf{k}|.$$

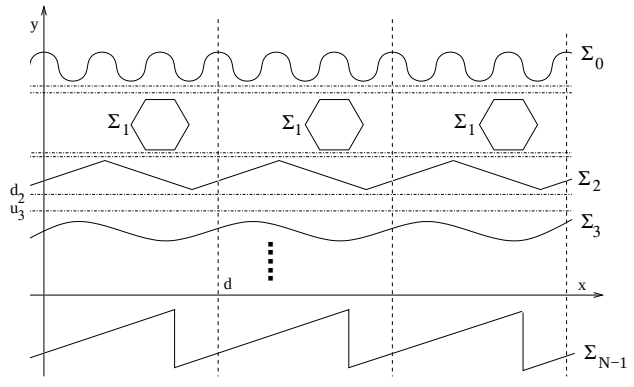

FIGURE 2. Cross section of a grating with separated boundaries.

If $\mathbf{k} = (0, -k, 0)$, we set $\mathbf{s} = (0, 0, 1)$ and hence $\mathbf{p} = (1, 0, 0)$. Then, the incident plane wave is given by its polarization angles

$$\delta = \arctan\big(|(\mathbf{E}^i, \mathbf{s})|/|(\mathbf{E}^i, \mathbf{p})|\big),\ \psi = -\arg\big((\mathbf{E}^i, \mathbf{s})/(\mathbf{E}^i, \mathbf{p})\big),$$

where $\delta \in [0, \pi/2]$, $\psi \in (-\pi, \pi]$. Since $\mathbf{E}^i$ is orthogonal to the wave vector, $(\mathbf{E}^i, \mathbf{k}) = 0$, one can decompose $\mathbf{E}^i$

$$\mathbf{E}^i = (\mathbf{E}^i,\ \mathbf{s})\,\mathbf{s} + (\mathbf{E}^i,\ \mathbf{p})\,\mathbf{p}.$$

It is easy to see that for incident and also diffracted field components $(\mathbf{E}, \mathbf{q})$ and $(\mathbf{E}, \mathbf{p})$ with propagation angles θ and ϕ and $\rho = \cos\phi(\sin^2\theta\cos^2\phi + \sin^2\phi)^{0.5}$

$$(\mathbf{E}, \mathbf{q}) = (E_z \sin\theta - B_z \cos\theta \sin\phi)/\rho,\ (\mathbf{E}, \mathbf{p}) = (E_z \cos\theta \sin\phi + B_z \sin\theta)/\rho,$$

where if $\mathbf{k} \parallel \nu$, then $(\mathbf{E}^i, \mathbf{q}) = E^i_z$ and $(\mathbf{E}^i, \mathbf{p}) = B^i_z$. The incident values (E^i_z, B^i_z) can be defined from these equations for the given incidence (θ, ϕ) and polarization (δ, ψ) angles under some normalization condition [30].

We seek a bounded H^1-regular solution (E_z, B_z) which is: α-quasi-periodic in x ($u(x + d), y) = \mathrm{e}^{\,\mathrm{i}\alpha d} u(x, y)$) and satisfies the radiation conditions

$$\begin{aligned}(E_z, B_z) &= (E^i_z, B^i_z) + \sum_{m\in\mathbb{Z}} (E^m_0, B^m_0)\mathrm{e}^{\,\mathrm{i}(\alpha_m x + \beta^m_0 y)} \quad \text{for } y \geq \sup\Sigma_0,\\ (E_z, B_z) &= \sum_{m\in\mathbb{Z}} (E^m_N, B^m_N)\mathrm{e}^{\,\mathrm{i}(\alpha_m x - \beta^m_N y)} \quad \text{for } y \leq \inf\Sigma_{N-1},\end{aligned} \tag{3}$$

where $\alpha_m = \alpha + 2\pi m/d$, $\beta^m_n = \sqrt{\omega^2\varepsilon_n\mu_n - \gamma^2 - \alpha^2_m}$ with $0 \leq \arg\beta^m_n < \pi$. In the following it is always assumed that besides $\varepsilon_0, \mu_0 > 0$

$$0 \leq \arg\varepsilon, \arg\mu \leq \pi, \arg(\varepsilon\mu) < 2\pi\,,$$

which holds for all existing optical (meta)materials [24]. Then the electromagnetic formulation of conical diffraction on multi-boundary gratings is equivalent to (1)–(3) for (E_z, B_z).

2.2. **S-matrix approach.** Since the grating profiles are strictly separated the problem (1)–(3) can be treated using certain robust algorithms for modeling layered gratings [an overview is given, for example, in Ref. 32]. The present method extends the S-matrix algorithm given in Ref. 33 for the integral method and the in-plane case. As we know, the first description of the scattering amplitude matrices algorithm has been done in Ref. 34. Its application to the off-plane case is described in Refs. 28 and 31. Here we give an exact description of the S-matrix algorithm combined effectively with the conical integral equations formulated for solving such multilayer grating problems.

Between surfaces Σ_{n-1} and Σ_n for all $n = 1, ..., N$ there exist strips $\{u_n < y < d_{n-1}\}$ which are not crossing the interfaces for $n = 1, ..., N$ (Fig. 2). In any strip $\{u_n < y < d_{n-1}\}$ with the cut wavenumber κ_n the solution (E_z, B_z) has the series expansion

$$(E_z, B_z) = \sum_{m\in\mathbb{Z}} \Big((a^m_n, c^m_n)\mathrm{e}^{\,\mathrm{i}\beta^m_n y} + (b^m_n, d^m_n)\mathrm{e}^{\,-\mathrm{i}\beta^m_n y}\Big)\mathrm{e}^{\,\mathrm{i}\alpha_m x}.$$

Let $y_n \in (u_n, d_{n-1})$ and denote

$$\begin{aligned}(A^m_n, C^m_n) &= \mathrm{e}^{\,-\mathrm{i}\beta^m_n y_n}(a^m_n, c^m_n), \quad (\mathcal{A}^m_n, \mathcal{C}^m_n) = \mathrm{e}^{\,-\mathrm{i}\beta^m_{n+1} y_n}(a^m_{n+1}, c^m_{n+1}),\\ (B^m_n, D^m_n) &= \mathrm{e}^{\,-\mathrm{i}\beta^m_n y_n}(b^m_n, d^m_n), \quad (\mathcal{B}^m_n, \mathcal{D}^m_n) = \mathrm{e}^{\,-\mathrm{i}\beta^m_{n+1} y_n}(b^m_{n+1}, d^m_{n+1}).\end{aligned}$$

Then in the strip $\{u_n < y < d_{n-1}\}$ above Σ_n

$$(E_z, B_z) = \sum_{m\in\mathbb{Z}} \Big((A^m_n, C^m_n)\mathrm{e}^{\,\mathrm{i}\beta^m_n (y - y_n)} + (B^m_n, D^m_n)\mathrm{e}^{\,-\mathrm{i}\beta^m_n (y - y_n)}\Big)\mathrm{e}^{\,\mathrm{i}\alpha_m x}$$

and in the strip $\{u_{n+1} < y < d_n\}$ below Σ_n

$$(E_z, B_z) = \sum_{m\in\mathbb{Z}} \Big((\mathcal{A}_n^m, \mathcal{C}_n^m) \mathrm{e}^{\,\mathrm{i}\beta_{n+1}^m (y-y_n)} + (\mathcal{B}_n^m, \mathcal{D}_n^m) \mathrm{e}^{\,-\mathrm{i}\beta_{n+1}^m (y-y_n)} \Big) \mathrm{e}^{\,\mathrm{i}\alpha_m x}$$

with amplitudes of incoming A_n, $\mathcal{B}_n$ and diffracted B_n, $\mathcal{A}_n$ waves defined as

$$A_n = \{(A_n^m, C_n^m)\}_{m\in\mathbb{Z}}, \quad \mathcal{B}_n = \{(\mathcal{B}_n^m, \mathcal{D}_n^m)\}_{m\in\mathbb{Z}},$$
$$B_n = \{(B_n^m, D_n^m)\}_{m\in\mathbb{Z}}, \quad \mathcal{A}_n = \{(\mathcal{A}_n^m, \mathcal{C}_n^m)\}_{m\in\mathbb{Z}}.$$

The multi-profile problem (1)–(3) is solved if the scattering amplitude columns B_0 and $\mathcal{A}_{N-1}$ are expressed for given input A_0 and vanishing $\mathcal{B}_{N-1}$. The S-matrix method looks for a recursion of operators R_j, T_j such that

$$B_n = R_n A_n\,,\ \mathcal{A}_{N-1} = T_n A_n\,, \quad n = N-1, \dots, 0.$$

The scattering amplitude columns are connected by two types of relations

$$\mathcal{A}_{n-1} = \gamma_n^{-1} A_{n-1},\ \mathcal{B}_{n-1} = \gamma_n B_n, \quad \gamma_n = \mathrm{diag}\{\exp(\mathrm{i}\beta_n^m (y_{n-1} - y_n)\}_{m\in\mathbb{Z}},$$
$$B_n = r_n A_n + t'_n \mathcal{B}_n,\ \mathcal{A}_n = t'_n A_n + r'_n \mathcal{B}_n,$$

where r_n or r'_n and t_n or t'_n are reflection and transmission operators, respectively, for the illumination of Σ_n from the above or below. This leads to a simple recursion starting from below

$$\begin{aligned} R_{n-1} &= r_{n-1} + t'_{n-1}\gamma_n R_n (I - \gamma_n r'_{n-1}\gamma_n R_n)^{-1}\gamma_n t_{n-1}, \\ T_{n-1} &= T_n (I - \gamma_n r'_{n-1}\gamma_n R_n)^{-1}\gamma_n t_{n-1}, \end{aligned} \tag{4}$$

with the unity operator I and initial values

$$R_{N-1} = r_{N-1}, T_{N-1} = t_{N-1}.$$

Finally one gets the desired amplitude vectors

$$B_0 = R_0 A_0\,,\ \mathcal{A}_{N-1} = T_0 A_0\,. \tag{5}$$

It is worth noting that the recursion is stable, since the elements of γ_n have norms ≤ 1, and can be used for any number of closed and continuous boundaries having any conductivity.

2.3. **Integral equations.** The reflection and transmission operators r_n, r'_n, t_n and t'_n of a given profile Σ_n, which separates two domains, are obtained from the response of that one-profile grating illuminated by plane waves from above and below. For definiteness we label the domains G_n and G_{n+1} and the corresponding material coefficients ε_n, μ_n and $\varepsilon_{n+1}, \mu_{n+1}$. If the surface Σ_n is continuous, then G_{n+1} denotes the domain below Σ_n, whereas for closed boundary profiles the domain G_{n+1} denotes one of the inclusions inside Σ_n. For off-plane diffraction one has to find the Rayleigh coefficients of the diffracted fields for input waves with z-components

$$\begin{pmatrix} E_\delta^+ \\ B_\delta^+ \end{pmatrix} = \begin{pmatrix} 1-\delta \\ \delta \end{pmatrix} \mathrm{e}^{\,\mathrm{i}(\alpha_m x - \beta_n^m y)}, \ \ \delta = 0, 1,$$

incident from above and

$$\begin{pmatrix} E_\delta^- \\ B_\delta^- \end{pmatrix} = \begin{pmatrix} 1-\delta \\ \delta \end{pmatrix} \mathrm{e}^{\,\mathrm{i}(\alpha_m x + \beta_{n+1}^m y)} \text{ or } \begin{pmatrix} E_\delta^- \\ B_\delta^- \end{pmatrix} = \begin{pmatrix} 1-\delta \\ \delta \end{pmatrix} \mathrm{e}^{\,\mathrm{i}(\alpha_m x + \beta_n^m y)}, \ \ \delta = 0, 1,$$

incident from below for continuous Σ_n or inclusions, respectively. For illumination from above one has to solve the following problem: Setting

$$E_z = \begin{cases} u_n + E_\delta^+, \\ u_{n+1}, \end{cases} \quad B_z = \begin{cases} v_n + B_\delta^+ & \text{in} \quad G_n, \\ v_{n+1} & \text{in} \quad G_{n+1}, \end{cases}$$

find α-quasiperiodic solutions of the Helmholtz equations

$$\big(\Delta + (\omega\kappa_n)^2\big)u_n = \big(\Delta + (\omega\kappa_n)^2\big)v_n = 0\,, \tag{6}$$

$$\big(\Delta + (\omega\kappa_{n+1})^2\big)u_{n+1} = \big(\Delta + (\omega\kappa_{n+1})^2\big)v_{n+1} = 0\,, \tag{7}$$

where now $\kappa_n^2 = \varepsilon_n\mu_n - \varepsilon_0\mu_0\sin^2\phi$. From equation (2) one gets the jump conditions on Σ_n

$$\begin{aligned}
&u_{n+1} = u_n + E_\delta^+\,,\ v_{n+1} = v_n + B_\delta^+\,,\\
&\frac{\varepsilon_{n+1}\,\partial_\nu u_{n+1}}{\kappa_{n+1}^2} - \frac{\varepsilon_n\partial_\nu(u_n + E_\delta^+)}{\kappa_n^2} = \frac{\varepsilon_0\sin\phi(\kappa_{n+1}^2 - \kappa_n^2)}{\kappa_n^2\kappa_{n+1}^2}\,\partial_t v_{n+1}\,,\\
&\frac{\mu_{n+1}\partial_\nu v_{n+1}}{\kappa_{n+1}^2} - \frac{\mu_n\partial_\nu(v_n + B_\delta^+)}{\kappa_n^2} = -\frac{\mu_0\sin\phi(\kappa_{n+1}^2 - \kappa_n^2)}{\kappa_n^2\kappa_{n+1}^2}\,\partial_t u_{n+1}\,.
\end{aligned}$$

For illumination from below we set

$$E_{\rm z} = \begin{cases} u_n, \\ u_{n+1} + E_\delta^-, \end{cases} \quad B_{\rm z} = \begin{cases} v_n & \text{in } G_n, \\ v_{n+1} + B_\delta^- & \text{in } G_{n+1}. \end{cases}$$

The α-quasiperiodic functions u_j, v_j have to satisfy the Helmholtz equations (6), (7) and the transmission conditions

$$\begin{aligned}
&u_{n+1} + E_\delta^- = u_n\,,\ v_{n+1} + B_\delta^- = v_n\,,\\
&\frac{\varepsilon_{n+1}\,\partial_\nu(u_{n+1} + E_\delta^-)}{\kappa_{n+1}^2} - \frac{\varepsilon_n\partial_\nu u_n}{\kappa_n^2} = \frac{\varepsilon_0\sin\phi(\kappa_{n+1}^2 - \kappa_n^2)}{\kappa_n^2\kappa_{n+1}^2}\,\partial_t v_n\,,\\
&\frac{\mu_{n+1}\partial_\nu(v_{n+1} + B_\delta^-)}{\kappa_{n+1}^2} - \frac{\mu_n\partial_\nu v_n}{\kappa_n^2} = -\frac{\mu_0\sin\phi(\kappa_{n+1}^2 - \kappa_n^2)}{\kappa_n^2\kappa_{n+1}^2}\,\partial_t u_n\,.
\end{aligned}$$

The solution of these general one-boundary conical diffraction problems is derived by using a combination of the direct (Green's formula) and indirect (via layer potentials) boundary integral approaches. In G_{n+1} the functions u_{n+1}, v_{n+1} are represented as single layer potentials with densities w, τ on Γ_n, denoting one period of Σ_n,

$$u_{n+1}(P) = \int_{\Gamma_n} w(Q)\,\Psi_{\kappa_{n+1}}(P-Q)\,d\sigma_Q, \quad v_{n+1}(P) = \int_{\Gamma_n} \tau(Q)\,\Psi_{\kappa_{n+1}}(P-Q)\,d\sigma_Q,$$

where $P = (X, Y)$ and $d\sigma_Q$ denotes the integration with respect to the arc length. The integral kernel $\Psi_{\kappa_{n+1}}$ is the α-quasi-periodic fundamental solution of period d with logarithmic singularities at points $\{(md, 0)\}$ given by the infinite series

$$\Psi_{\kappa_{n+1}}(P) = \frac{i}{4}\sum_{m=-\infty}^{\infty} H_0^{(1)}\Big(\omega\kappa_{n+1}\sqrt{(X-md)^2 + Y^2}\Big)\,{\rm e}^{\,imd\alpha},$$

where $H_0^{(1)}$ is the first Hankel function of zero order. Based on the known jump relations for layer potentials one concludes as in Ref. 18 that the transmission conditions on Σ_n are fulfilled only if the functions w, τ are solutions of the system of integral equations

$$\begin{aligned}
&\frac{\varepsilon_{n+1}\kappa_n^2}{\varepsilon_n\kappa_{n+1}^2}V_n(L_{n+1} - I)w - (I + K_n)\,V_{n+1}w + \varepsilon_0\sin\phi\Big(1 - \frac{\kappa_n^2}{\kappa_{n+1}^2}\Big)H_n V_{n+1}\tau = \mathcal{U},\\
&\frac{\mu_{n+1}\kappa_n^2}{\mu_n\kappa_{n+1}^2}V_n(L_{n+1} - I)\tau - (I + K_n)\,V_{n+1}\tau - \mu_0\sin\phi\Big(1 - \frac{\kappa_n^2}{\kappa_{n+1}^2}\Big)H_n V_{n+1}w = \mathcal{V}
\end{aligned} \tag{8}$$

with righthand sides $\mathcal{U}$ and $\mathcal{V}$ determined by the input waves $E_\delta^\pm$ and $B_\delta^\pm$. Here the integral operators V_n, K_n are the single and double layer potentials

$$V_n\varphi(P) = 2\int_{\Gamma_n} \varphi(Q)\,\Psi_{\kappa_n}(P-Q)\,d\sigma_Q, \quad K_n\varphi(P) = 2\int_{\Gamma_n} \varphi(Q)\,\partial_{\nu(Q)}\Psi_{\kappa_n}(P-Q)\,d\sigma_Q,$$

with $P \in \Sigma_n$ and $\nu(Q)$ is the normal to Σ_n at Q pointing into G_{n+1}. These boundary integral operators as well as the adjoint of the double layer potential

$$L_n\varphi(P) = 2\int_{\Gamma_n} \varphi(Q)\,\partial_{\nu(P)}\Psi_{\kappa_n}(P-Q)\,d\sigma_Q$$

appear already in integral methods for classical diffraction. The presence of tangential derivatives in the jump conditions for solutions of conical diffraction leads to a new boundary integral

$$H_n\varphi(P) = 2\int_{\Gamma_n} \varphi(Q)\,\partial_{t(Q)}\Psi_{\kappa_n}(P-Q)\,d\sigma_Q.$$

Since the kernel of this integral operator is strongly singular, $H_n\varphi$ has to be interpreted as principal value integral and therefore (8) represents a system of singular integral equations.

Properties of this system are described in Refs. 18, 24 for the case of incident plane waves from above, where one gets

$$\mathcal{U} = -2E_\delta^+,\ \mathcal{V} = -2B_\delta^+\,,$$

as righthand sides of (8). Analogously, for illumination from below the transmission conditions on Σ_n lead to the righthand sides

$$\mathcal{U} = \frac{\varepsilon_{n+1}\kappa_n^2}{\varepsilon_n\kappa_{n+1}^2}V_n\partial_\nu E_\delta^- - (I+K_n)\,E_\delta^- + \varepsilon_0\sin\phi\Big(1-\frac{\kappa_n^2}{\kappa_{n+1}^2}\Big)H_nB_\delta^-,$$
$$\mathcal{V} = \frac{\mu_{n+1}\kappa_n^2}{\mu_n\kappa_{n+1}^2}V_n\partial_\nu B_\delta^- - (I+K_n)\,B_\delta^- - \mu_0\sin\phi\Big(1-\frac{\kappa_n^2}{\kappa_{n+1}^2}\Big)H_nE_\delta^-.$$

in case of a continuous profile and

$$\mathcal{U} = -2E_\delta^-,\ \mathcal{V} = -2B_\delta^-$$

for closed boundary profiles.

The advantage of our integral formulation (4)–(8) is a clever combination of the integral equations with the S-matrix algorithm allowing one to solve the single discrete problem for computing scattering amplitude matrices of (4). As a result, the computation of the discrete matrix on the left of (8) and its factorization have to be performed only once for that profile due to the unified treatment of different incoming waves.

3. Numerical implementation

We discuss briefly the numerical solution of systems (4)–(8). In the computations the indices $m \in [M_0, M_1]$ are chosen such that at least all propagating modes for all one-profile gratings are covered, i.e. we require that $\beta_n^m \notin \mathbb{R}$ for all $m \notin [M_0, M_1]$ and n. Thus, by solving (8) for $M = 2(M_1 - M_0 + 1)$ incident waves E_δ^+, B_δ^+ and computing the scattering amplitudes for all modes $m \in [M_0, M_1]$ of u_n, v_n and u_{n+1}, v_{n+1} we derive $M \times M$ reflection and transmission matrices r_n and t_n for illumination from the above. Analogously, the $M \times M$ reflection and transmission matrices r_n' and t_n' are obtained from (8) with M incident waves E_δ^-, B_δ^-, illuminating the profile from the below. These reflection and transmission matrices for each boundary profile are computed simultaneously as described above.

The kernels of the integrals V_n have a logarithmic singularity like $\log|s-t|$ and H_n is a singular integral operator with the kernel singularity $1/(s-t)$ as $t \to s$. Therefore the discretization of the integrals requires some caution, especially if the profile has corners, where additionally the kernels of K_n and L_n have fixed singularities. The integral equations are discretized with a collocation method, the unknowns are sought as trigonometric polynomials which in the case of gratings with edges are partially replaced by splines to improve the approximation of the solution near the profile corners [18]. The trigonometric collocation method with special treatment of singular integrals gives for smooth boundary profiles with the number of collocation points $\mathcal{N}$ the convergence rate of order $O(\mathcal{N}^{-3})$. The hybrid trigonometric-spline collocation with mesh grading near corners gives the convergence rate of order $O(\mathcal{N}^{-2})$.

Expressions (4) allow us to find amplitude matrices by a recursive procedure beginning with the lower medium. To do this, we have to know, in a general case, four matrices of scattering amplitudes and perform two matrix inversions in each iteration step. The computation time for one-boundary problems was shown to scale quadratically with the main accuracy parameter (the number of collocation points) [18]. The computation time is also linearly proportional to the number of boundaries. Using Hankel functions as fundamental solutions for closed boundaries decreases the number of required collocation points in several times. The memory cache for amplitude matrices of multi-layer grating problems (e.g. photonic crystals) with the same boundary profiles and the same pairs or quads of layers can be used.

The code developed and tested is found to be accurate and efficient for solving various in-plane and off-plane diffraction problems, including high-conductive gratings, surfaces with edges, real groove profiles, and gratings with non-function boundary profiles. Extension to rod gratings and two-dimensional PBGs is naturally obtained. The high rate of convergence, the high accuracy, and the short computation time of the suggested solver are further demonstrated for various non-trivial numerical examples.

4. Computation of PBG examples in sensitive cases

The workability of the code developed has been confirmed by numerous tests usually employed in classical and conical diffraction cases, more specifically: the reciprocity theorem; stabilization of results under doubling of the number of collocation points and variation of the calculation accuracy of

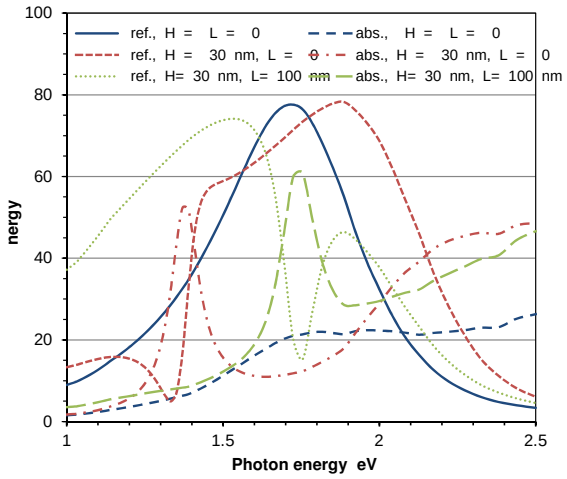

FIGURE 3. Calculated reflection and absorption spectra of SiO_2-embedded $d = 200$-nm gratings with Au nanowires of 100×15 nm^2 rectangular cross section and different vertical, H, and horizontal, L, displacements are plotted vs. photon energy for normal incidence and TM polarization.

kernel functions; comparison with analytically amenable cases of plane interfaces; consideration of the inverse (non-physical) radiation condition; use of different variants of collocation point distribution on boundaries (mesh refinements); comparison with the results obtained by another of our codes or with published data, or with information submitted to us by other researchers, including results of measurements. A small part of such numerical tests devoted to the analysis of sensitive cases of various PBGs is demonstrated in this Section. The presented results demonstrate the impact of rod shape on diffraction in PBGs supporting polariton-plasmon excitation and other types of anomalies (i.e. waveguiding anomalies, cavity modes, Fabry-Perot resonances, Rayleigh orders, etc), particularly in the vicinity of resonances and at high filling ratios. In conical diffraction, the influence of all possible types of waves can be mixed.

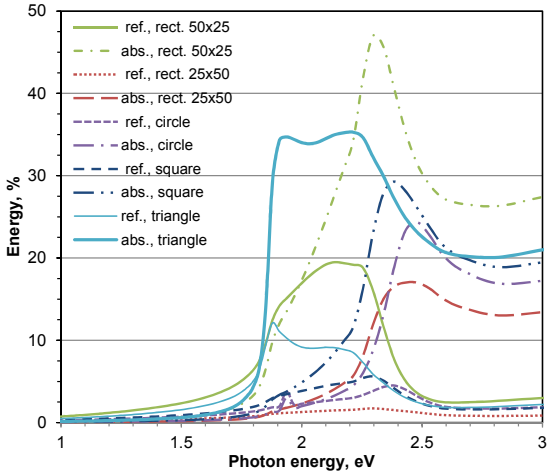

FIGURE 4. Calculated reflection and absorption spectra of SiO_2-embedded $d = 200$-nm gratings with Au nanowires of different cross section, the same area of $\mathcal{S} = 1250$ nm^2, and $H = L = 0$ ($N - 1 = 1$) are plotted vs. photon energy for normal incidence and TM polarization.

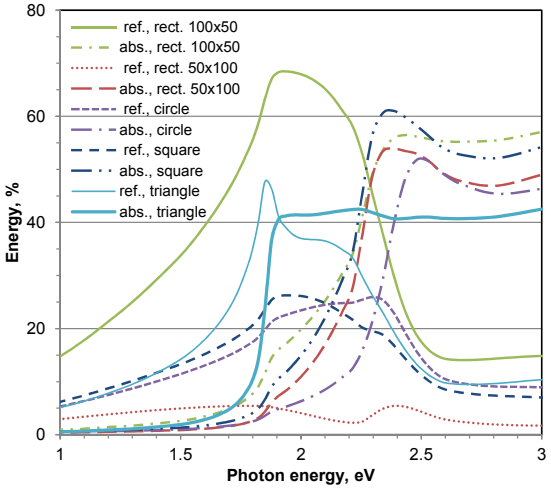

FIGURE 5. The same as in Figure 4, but for the same nanowire cross section area of $\mathcal{S} = 5000$ nm^2.

4.1. **PBGs with nano-rods supporting polariton-plasmon excitation.** In this Subsection, we are going to analyze numerically the optical response of photonic crystal slabs supporting polariton-plasmon excitation with different cross sections of nanowires invariant with respect to the z axis and different number of gratings stacked one upon the other. As far as we know from publications, there is

no detailed description of the influence of very different rod geometries and of the filling factor on PBGs with nanowires supporting polariton-plasmon excitation. The model contains $N-1$ identical gratings of arbitrary cross section displaced vertically (by H_n) and horizontally (by L_n) relative to one another and embedded in a homogeneous medium with dielectric permittivity ε_1 and magnetic susceptibility μ_1. We are going to deal here only with materials with $\mu_n = 1$, although the model is applicable to other cases as well, including metamaterials [18]. The dependence of the dielectric permittivity ε_2 of the material of nanorods on the incident photon frequency is assumed to be known. The lower medium (substrate) and the upper one are likewise assigned pairs of material constants, but one may conceive of more complicated cases of multi-layer structures as well. The model allows also arbitrary incidence of, in the general case, elliptically polarized radiation on PBGs, which is prescribed by two angles of incidence and two angles of polarization.

In Fig. 3, calculated spectra of reflected energy for PBGs with Au nanowires of rectangular cross section, measuring 100×15 nm^2 and $N-1=1$ ($H=L=0$) or $N-1=2$ ($H=30$ nm, $L=0$ and $H=30$ nm, $L=100$ nm) are compared with similar spectra derived in [35] (Fig. 3a in Ref. 35) by the PWE approach. We consider here TM-polarized radiation (the plane of polarization is perpendicular to the lines) incident normally with respect to the x-z plane) on a grating with a period $d=200$ nm and refractive indices of Au taken from [36]. To eliminate interference effects, the Au nanorods are embedded in an infinite homogeneous fused silica matrix with dielectric permittivity $\varepsilon_{0,1,3}=2.13$. Examining the two figures, we see a very good agreement, which evidences applicability of both rigorous numerical methods to analysis of diffraction on such PBGs with rectangular slabs.

Figure 4 displays for comparison theoretical spectra of energy reflected from, and absorbed by, a PBG with Au nanowires of circular, square, rectangular, and triangular cross sections of the same area and with $N-1=1$ studied in the 1−3-eV range (visible and near infra-red). In this and subsequent examples we consider the TM- polarized light normally falling on Au nanowires embedded in a SiO_2 matrix with $d=200$ nm and refractive indices of Au taken from [37]. The orientation of the rods having edges is chosen in such a way that light normally falls on one side of the rods only. The $a \times b$ dimensions of the rectangular rods selected for this example are 50×25 nm^2 or 25×50 nm^2 and the width of the squares or triangles and diameter of the circles were chosen to obtain equal cross sectional area $\mathcal{S}=1250$ nm^2. As seen from Fig. 4, reflection and, particularly, absorption spectra exhibit a strong difference near the plasmon-polariton anomaly among the five shapes of

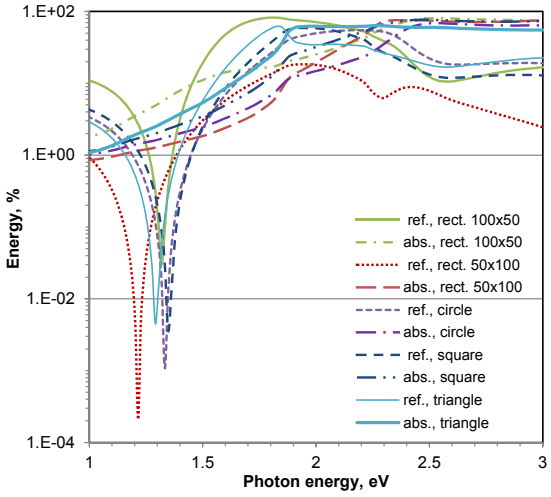

FIGURE 6. Calculated reflection and absorption spectra of SiO_2-embedded $d=200$-nm gratings with Au nanowires of different cross section, the same area $\mathcal{S}=5000$ nm^2, and $N-1=2$, $H=50$ nm, $L=0$ are plotted vs. photon energy for normal incidence and TM polarization.

the nanowire cross section chosen. These differences amount to several hundred percent for the rectangles because of their different width-to-height ratio (two and a half) compared with the square or the circle (one) and the equilateral triangle (0.866). One observes also a noticeable difference in the positions of the absorption and reflection maxima among different grating profiles. Thus, the simple effective medium theory cannot be applied to design and analysis of such PBGs, even for a small filling ratio.

Figure 5 presents energy spectra similar to those displayed in Fig. 4 but for $\mathcal{S}$ four times that of the preceding example. In this case, $a \times b = 100 \times 50$ nm^2 or 50×100 nm^2. We readily see that the differences in the reflection and absorption spectra among gratings of different profiles increase with increasing filling ratio and are observed now not only close to the plasmon resonances. Near the resonances, they amount to a few tens of percent of energy (Fig. 5). The absorption spectra of the triangular-shaped nanowires have an interesting band-gap-like structure that is not the case for absorption spectra of nanowires of other rod shapes.

Figure 6 shows spectra similar to those depicted in Fig. 5 but for $N-1=2$, $H=50$ nm, and $L=0$. In the case of two gratings, the plasmon-polariton resonance frequencies are subtracted or summed [35], and one may expect still larger differences in the spectra of reflected and absorbed energy among crystals with lattice cells of different shape. Indeed, Fig. 6 drawn on a log scale reveals enormous differences, up to orders of magnitude, throughout the spectrum studied. The minimum reflectance of $\sim 10^{-6}$ is observed for a photonic bandgap with a rectangular cross section of 100×50 nm^2. The positions of the reflection minima are also very different for different rod shapes.

Only $\mathcal{N} = 50$ and mesh grading were used to compute these examples which allocate ~ 0.1 MB memory. The relative error calculated from the energy balance for absorption gratings is $\sim 10^{-4}$. The average time taken up by one point on a portable workstation IBM® ThinkPad® R50p with an Intel® Pentium® M 1.7 GHz processor and 2 GByte of RAM is ~ 0.1 sec only when operating on Linux (kernel 2.6.17).

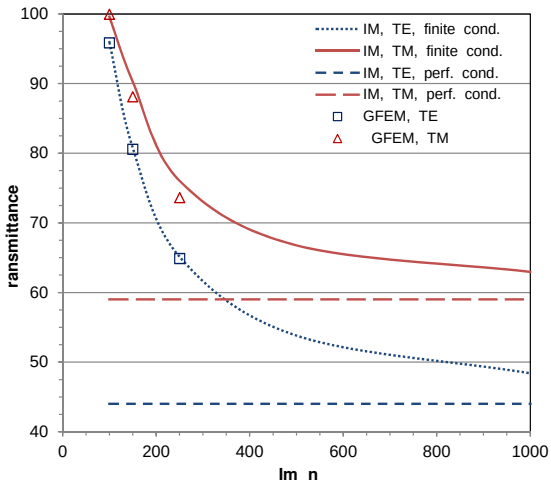

FIGURE 7. TE and TM transmittances of a $d = 10$-mm grating with high-conductive rectangular rods of 7×1 mm^2 cross section, which are embedded in a matrix with $n_0 = 3.47$, $N-1=2$, $H=1$ mm, and $L=0$, are plotted vs. $\mathrm{Im}\,[n]$. Calculations were performed for normal incidence at $\lambda = 15.24$ mm.

4.2. **PBGs with high-conductive rods supporting waveguide modes.** As it has been demonstrated in the previous example, owing to the existence of surface plasmon resonance, even a single-grating structure could almost totally transmit TM polarization (Figs. 3–6). One can exclude the influence of plasmon surface waves using a grating structure in the TE polarization, for which plasmons cannot propagate, and investigate the role of waveguide modes and Fabry-Perot resonances.

Figure 7 displays transmission TE and TM spectra for PBGs with high-conductive lossless ($\mathrm{Re}\,[n_2] = 0$) rectangular rods of 7×1 mm^2 with $d = 10$ mm embedded in matrix with $n_1 = 3.47$ for $N-1 = 2$, $H = 1$ mm, and $L = 0$ at $\lambda = 15.24$ mm. The outermost media have refractive index $n_{0,3} = 1$. Very similar spectra were calculated in Ref. 38 (Fig. 10(a)) by the CWM for the TE polarization and $\mathrm{Im}\,[n_2] = 250$ only. In addition, the efficiency simulation data based on the present IM were cross-checked in both polarization states against the rigorous Generalized Finite Element Method (GFEM) [39], in order to verify the reliability of the results obtained. The grating efficiencies calculated with two different approaches mentioned above are in a good agreement for all compared $\mathrm{Im}\,[n_2]$ data. Obviously enough, the difference between the transmittance values calculated by the two independent codes is bigger for the TM polarization state and higher $\mathrm{Im}\,[n_2]$. So the applicability of the IM and GFEM to analyse both TE and TM diffraction on such PBGs for high values of the imaginary part of the refractive index of rods is demonstrated. One can also compare the absolute efficiencies of this example with values predicted by the perfect conductivity model (Fig. 7). The asymptotic transmittance data calculated by using that model are $\sim 44\%$ (TE) and $\sim 59\%$ (TM). Interestingly, even at a very high value of $\mathrm{Im}\,[n_2] = 1000$ the results obtained for the finite conductivity model differ significantly from those obtained for the perfect conductivity model.

For this very hard-to-solve example (we do not know any rigorous numerical method that can do computations for $\mathrm{Re}\,[n_2] = 0$ and $\mathrm{Im}\,[n_2] = 1000$) we will examine the convergence rate and the accuracy of the prediction of reflection and transmission energies and absorption with respect to $\mathcal{N}$. For the efficiency convergence testing, the magnitude of computational errors cannot be reliably deduced from accuracy criteria based on a single computation such as the energy balance or the inverse radiation condition tests. For this purpose comparative studies should be used, i.e., $\mathcal{N}$-doubling [18]. As it can be seen from Fig. 8, the IM transmittance values for $\mathrm{Im}\,[n_2] = 250$ and $\mathrm{Im}\,[n_2] = 500$ stabilize, and the convergence is starting at $\mathcal{N} = 500$ (TE) and $\mathcal{N} = 1000$ (TM) and achieved with high accuracy at $\mathcal{N} = 1000$ (TE) and $\mathcal{N} = 2000$ (TM). The absolute differences between the values

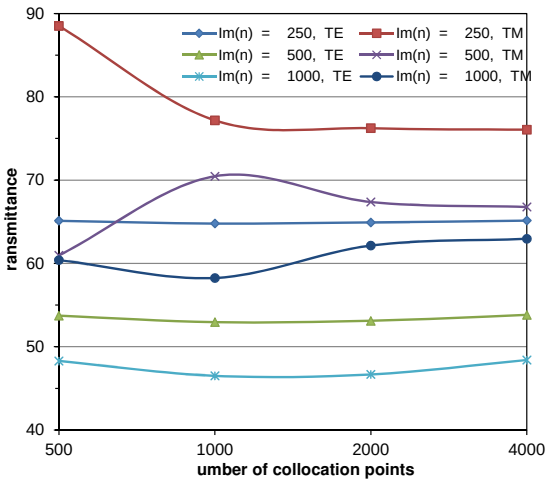

FIGURE 8. TE and TM transmittances of a $d = 10$-mm grating with high-conductive rectangular rods of 7×1 mm^2 cross section, which are embedded in matrix with $n_0 = 3.47$, $N-1 = 2$, $H = 1$ mm, and $L = 0$, are plotted vs. number of collocation points. Calculations were performed for normal incidence at $\lambda = 15.24$ mm.

calculated for $\mathcal{N} = 1000$ and $\mathcal{N} = 4000$ in the transmission energies for $\mathrm{Im}\,[n_2] = 250$ are 0.00353 for the TE polarization and 0.0111 for the TM one. Note that the energy balance errors are $\sim 10^{-5}$ and $\sim 10^{-6}$ for these values of $\mathcal{N}$, respectively. However, transmittance values for the hard case of $\mathrm{Im}\,[n_2] = 1000$ stabilize at $\mathcal{N} = 4000$ only. Thus, the convergence rate is high enough, taking into account the very difficult cases tested.

The computation time for a point calculated with ($\mathcal{N} = 2000$) is ~ 30 sec on the above mentioned PC, and the required RAM is ~ 1 GB. In this case the use of graded meshes gave the most accurate results compared with data obtained by applying other computational options.

4.3. **PBGs with dielectric rods supporting Bragg diffraction.** In this example we consider numerically some diffraction properties of non-absorbing PBGs with dielectric rods. The influence of the geometry and number of crystal layers, the shape of rods, the filling ratio, the index of refraction of materials and the polarization and diffraction angles of light can be investigated for this type of PBGs. The vital role of the filling ratio, refractive index, and polarization was demonstrated for the classical

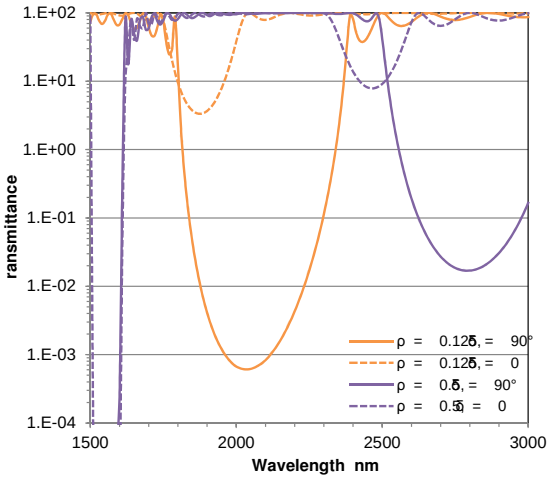

FIGURE 9. Calculated transmission spectra of a $d = 1\,\mu$m grating with dielectric circular rods with $n_2 = 3.47$ and filling ratio ρ embedded in vacuum with $N-1 = 15$, $H = 0.866\,\mu$m, and $L = 0.5\,\mu$m, are plotted vs. wavelength of incidence radiation with $\theta = 0$, $\phi = 0$ (classical diffraction), and polarization angle δ.

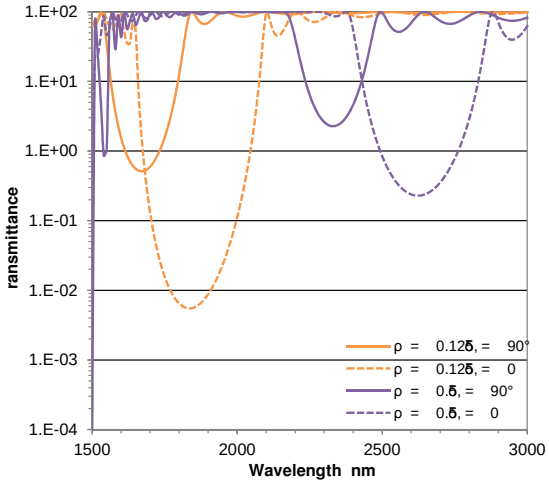

FIGURE 10. The same as in Figure 9, but for $\phi = 30°$ (conical diffraction).

diffraction [2, 33]. Here we demonstrate, as an example of possibilities of developed software, the vital role of the filling ratio and polarization for conical diffraction.

Figures 9 and 10 display spectral transmission for PBG circular rods with $d = 1\,\mu$m and $n_2 = 2$ embedded in vacuum at filling ratios of 0.125 and 0.5 for $N - 1 = 15$, $H = 0.866\,\mu$m, and $L = 0.5\,\mu$m (hexagonal crystal geometry) for $\theta = 0$, $\psi = 0$, and $\delta = 90^\circ$ (TE- or s-polarization) or $\delta = 0^\circ$ (TM- or p-polarization). In Fig. 9 one can see in-plane diffraction efficiencies ($\phi = 0$) and similar transmittance data computed in Ref. 33 by the boundary integral equation method (Figs. 6 and 11 of Ref. 33). In Fig. 10 for the off-plane diffraction $\phi = 30^\circ$ and this is an additional parameter compared with the classical diffraction case.

For both in-plane and off-plane examples there is a very different behavior in diffraction properties for the TE and TM polarizations of the incident radiation, especially for big filling ratios. Comparing with respective curves obtained in Figs. 9 and 10, it emerges that for s-polarized light the centers of the conical diffraction gaps have shifted significantly to smaller wavelengths and the widths and depths of the gaps have considerably decreased. In contrast to this behavior, for p-polarized light the centers of the conical diffraction gaps compared with the in-plane ones have shifted a little bit in opposite directions and the widths and depths of these gaps have considerably increased. The vital importance of the azimuthal angle ϕ as well as the incidence polarization has become evident even for a small filling ratio (0.125), however they are more important for a high filling ratio (0.5). Thus, using the conical diffraction for dielectric PBGs gives an additional control parameters which significantly affect Bragg diffraction and existing photonic band gaps.

Only $\mathcal{N} = 50$ without mesh grading are required to compute this example that allocate ~ 0.2 MB memory. The relative error calculated from the energy balance for non-absorption gratings is $\sim 10^{-4}$. The average time taken up by one point on the above mentioned PC is ~ 1 sec.

5. Summary and conclusions

The multi-layer integral-equation-based method is proposed to calculate the sensitive diffraction properties of PBGs with separated boundaries. It is possible to determine the diffracted field by computing the scattering matrices separately for various grating boundary profiles including dielectric, absorbing, and high-conductive rods working in any wavelength range. The computation of the matrices is based on the solution of a 2×2 system of singular integral equations at each interface between two different materials. The discretization of the integral equation system and the factorization of the discrete matrices (which takes the major computing time for one-boundary problems as well) have to be performed only once in order to compute these matrices for each boundary profile. It turned out that due to a high convergence rate a small number of collocation points per boundary combined with a high convergence rate can provide adequate description of the dependence on diffracted energy of very different PBGs illuminated at arbitrary incident and polarization angles.

In the present numerical analysis of the optical response of PBGs, a significant impact of rod shapes on diffraction supporting polariton-plasmon excitation, particularly in the vicinity of resonances and at high filling ratios has been investigated. The most sensitive rod shapes are rectangular and triangular due to their lower symmetry and special resonance features connected with edges. The diffracted energy response calculated vs. array cell geometry parameters was found to vary from a few percent up to a few hundred percent. The influence of other types of anomalies (i.e. waveguide anomalies, cavity modes, Fabry-Perot and Bragg resonances, Rayleigh orders, etc), conductivity, and polarization states has been demonstrated. Unexpectedly, the results obtained for the finite conductivity model of PBGs with high-conductive lossless ($\mathrm{Re}\,[n_2] = 0$) rectangular rods at very high values of $\mathrm{Im}\,[n_2]$ differ significantly from those obtained for the perfect conductivity model. The vital role of conical diffraction ($\phi \neq 0$) as well as the incident polarization has been demonstrated for PBGs with dielectric circular

rods supporting Bragg diffraction at different filling ratios. Thus, the rod and diffraction geometries, conductivity, and polarization cannot be ignored in many sensitive cases and simple and inaccurate theories cannot be applied to design and analysis of such complex PBGs. The multi-layer conical solver developed and tested is found to be very accurate and fast for solving PBG diffraction problems with high-conductive rods of arbitrary shapes, in particular with real boundary profiles, the case that should be studied experimentally. Due to a good convergence, the considered IM can be extended to handle 3D PBGs (2D multi-layer diffraction gratings) that will be addressed in future publications.

REFERENCES

[1] R. Petit, ed., *Electromagnetic theory of gratings*, (Springer, Berlin, 1980).
[2] K. Yasumoto, ed., *Electromagnetic Theory and Applications for Photonic Crystals*, (Taylor & Francis, Boca Raton, 2006).
[3] E. G. Loewen and E. Popov, *Diffraction Gratings and Applications* (Marcel Dekker, New York, 1997).
[4] M. Neviere and E. Popov, *Light Propagation in Periodic Media: Differential Theory and Design* (Marcel Dekker, New York, 2003).
[5] S. G. Johnson and J. D. Joannopoulos, *Photonic Crystals The Road from Theory to Practice* (Springer, New York, 2002).
[6] Website, http://www.ece.nus.edu.sg/stfpage/eleadj/ planewave.htm (2011).
[7] G. Kobidze, B. Shanker, and D. P. Nyquist, Phys. Rev. E **72**, 056702 (2005).
[8] A. Christ, T. Zentgraf, J. Kuhl, S. G. Tikhodeev, N. A. Gippius, and H. Giessen, Phys. Rev. B **70**, 125113 (2004).
[9] M. G. Moharam and T. K. Gaylord, J. Opt. Soc. Am. **71**, 811 (1981).
[10] B. Kleemann, A. Mitreiter, and F. Wyrowski, J. Mod. Opt. **43**, 1323 (1996).
[11] E. Popov, B. Chernov, M. Neviere, and N. Bonod, J. Opt. Soc. Am. A **21**, 199-206 (2004).
[12] E. Popov, M. Neviere, B. Gralak, and G. Tayeb, J. Opt. Soc. Am. A **19**, 33 (2002).
[13] M. A. Gilman, S. Yu. Sadov, A. S. Shamaev, and S. I. Shamaev, J. Comm. Tech. El. **45**, S229 (2000).
[14] V. A. Soifer, ed., *Methods for Computer Design of Diffractive Optical Elements* (Wiley, New York, 2002).
[15] A. Rathsfeld, G. Schmidt, and B. H. Kleemann, Commun. Comput. Phys. **1**, 984 (2006).
[16] L. I. Goray and S. Yu. Sadov, OSA Trends in Optics and Photonics Series **75**, 365 (2002).
[17] Website, http://www.pcgrate.com (2011).
[18] L. I. Goray and G. Schmidt, J. Opt. Soc. Am. A **27**, 585 (2010).
[19] B. H. Kleemann and J. Erxmeyer, J. Mod. Opt. **51**, 2093 (2004).
[20] L. I.Goray and J. F. Seely, Appl. Opt. **41**, 1434 (2002).
[21] L. I. Goray, J. F. Seely, and S. Yu. Sadov, J. Appl. Phys. **100**, 094901 (2006).
[22] L. I. Goray, J. Appl. Phys. **108**, 033516 (2010).
[23] Y. Wu and Y. Y. Lu, J. Opt. Soc. Am. A **28**, 1191 (2011).
[24] G. Schmidt, in *Around the Research of Vladimir Maz'ya II. Partial Differential Equations* (Springer, 2010), 337.
[25] L. I. Goray, Waves Random Media **20** 569 (2010).
[26] G. Schmidt, Appl. Anal. **82**, 75 (2003).
[27] J. Seely, B. Kjornrattanawanich, L. Goray, Y. Feng, and J. Bremer, Appl. Opt. **50**, 3015 (2011).
[28] G. Schmidt and B. H. Kleemann, J. Mod. Opt. **58**, 407 (2011).
[29] J. M. Taboada, J. Rivero, F. Obelleiro, M. G. Araujo, and L. Landesa, J. Opt. Soc. Am. A **28**, 1341 (2011).
[30] L. I. Goray and G. Schmidt, *Days on Diffraction (DD)*, 2009 Proceedings of the International Conference, 92 (2010).
[31] L. I. Goray, Proc. Soc. Photo-Opt. Instrum. Eng. **7390**, 73900V (2009).
[32] L. Li, J. Opt. Soc. Am. A **13**, 1024 (1996).
[33] D. Maystre, Pur. Appl. Opt. **3**, 975 (1994).
[34] S. A. Schelkunoff, Bell Syst. Tech. J. **17**, 17 (1938).
[35] A. Christ, Y. Ekinci, H. H. Solak, N. A. Gippius, S. G. Tikhodeev, and O. J. F. Martin, Phys. Rev. B **76**, 201405 (2007).
[36] P. B. Johnson and R. W. Christy, Phys. Rev. B **6**, 4370 (1972).
[37] E. D. Palik, ed., *Handbook of Optical Constant of Solids* (Academic, Orlando, 1985).
[38] E. Popov, S. Enoch, G. Tayeb, M. Neviere, B. Gralak, and N. Bonod, Appl. Opt. **43**, 999 (2004).
[39] J. Elschner, R. Hinder, A. Rathsfeld, and G. Schmidt, DIPOG Homepage, http://www.wias-berlin.de/software/DIPOG (2011).